## **RSC Advances**



## **PAPER**

View Article Online
View Journal | View Issue



Cite this: RSC Adv., 2020, 10, 32875

# All-organic, conductive and biodegradable yarns from core—shell nanofibers through electrospinning†

Vishakha T. Weerasinghe, D. G. Kanchana Dissanayake, Dawas W. Pamoda T. D. Perera, Dawas Nadeeka D. Tissera, Ruchira N. Wijesena and Nandula D. Wanasekara x

Electrically conductive and biodegradable materials are desired for a range of applications in wearable electronics to address the growing ecological problem of e-waste. Herein, we report on the design and fabrication of all-organic, conductive and biodegradable nanofibrous core–shell yarn produced by *in situ* polymerization of aniline on the surface of electrospun poly(ε-caprolactone) nanofibers. The effect of concentration of aniline monomer on the morphology and resistivity of deposited polyaniline layer was investigated. The electrical resistance changed almost instantaneously with the strain for multiple stretch and recovery cycles. This rapid and sensitive response to mechanical loading and unloading is promising to validate the possibility of using the conductive yarns as strain sensors for monitoring human motion. Increasing the number of plies of yarn to three resulted in a three-fold reduction of the resistance. The twisted plied yarns were incorporated into fabric by stitching to demonstrate their use as a wearable electrode for capacitive sensors. This approach presents an early step in realizing all-organic conductive biodegradable nanofibrous yarns for biodegradable smart textiles.

Received 21st June 2020 Accepted 24th August 2020

DOI: 10.1039/d0ra05430e

rsc.li/rsc-advances

#### Introduction

Smart textiles have attracted great interest in a range of fields such as healthcare, public safety, space exploration, consumer fitness and sport<sup>1,2</sup> with the use of antennas,<sup>3</sup> sensors<sup>4</sup> and electromagnetic interference shielding devices.<sup>5</sup> Nowadays, the most commercial applications of smart textiles are fabricated by integrating rigid conventional electronic hardware units into clothes.6 However, these devices have limited the desired properties of textiles such as breathability, flexibility and lightweight. Therefore, the field of wearable electronics is being revolutionized by integrating electronic functionalities directly into fabric, yarn or fiber.7 Conductive yarn is an important component of smart-textiles, which can be utilized as electrodes or connectors by weaving, knitting and/or stitching.8,9 Generally, conductive yarns are manufactured by embedding or coating inorganic materials such as carbon, silver, gold, nickel, and copper. Even though these composite yarns have superior

Conductive polymers have attracted much attention as the only choice for organic conductors and they exhibit interesting electronic, electrical, optical and magnetic properties. 12,13 Among an array of conductive polymers, polyaniline (PANI) has been popular owing to the good environmental and thermal stability, light-weight, optical properties, and high electrical conductivity.14,15 These polymers have been incorporated into wet-spun or electrospun yarns as a coating or a filler.16 Electrospinning is a robust process that is capable of producing nanofibre mats with a range of tunable properties such as fiber diameter, strength and porosity.17 Furthermore, electrospinning provides the ability to produce ultrathin aligned or non-aligned fiber webs or continuous nanofibrous yarns with excellent mechanical properties and high surface area. 18,19 The high conductivity coupled with large specific surface area provides an excellent platform to fabricate capacitive and resistive sensors.20,21

The development of conductive yarns from PANI coated or blended polyacrylonitrile (PAN) electrospun yarns<sup>22,23</sup> and polyethylene terephthalate (PET) melt spun yarns have been reported.<sup>14</sup> However, with the increased attention to sustainable

conductivity, the inorganic component may lead to several drawbacks such as chemical corrosion, low-strength, sloughing of deposition, stiff feeling, easy decay<sup>10</sup> and limitations of processability. The use of organic conductive polymers with a range of properties offer a better alternative to impart conductivity to smart textiles.<sup>11</sup>

<sup>&</sup>lt;sup>a</sup>University of Moratuwa, Bandaranayake Mawatha, Moratuwa 10400, Sri Lanka. E-mail: nandulad@uom.lk

<sup>&</sup>lt;sup>b</sup>Sri Lanka Institute of Nanotechnology (SLINTEC), Nanotechnology and Science Park, Mahenwatte, Pitipana, Homagama 10200, Sri Lanka

<sup>†</sup> Electronic supplementary information (ESI) available: PANI polymerization, schematic diagram of test circuit for conductivity measurement, homemade apparatus for measuring resistance  $\nu s$ . strain, woven and sewn yarn, SEM of degraded fibers. See DOI: 10.1039/d0ra05430e

textile production routes, PAN and PET polymers do present with problems in disposal due to non-biodegradability. Waste prevention in the design stage is an initial strategy than recycling or end of life treatments. Piological Biodegradable materials such as poly(ethylene-co-vinyl acetate), poly(lactic acid) (PLA), poly(ecaprolactone) (PCL), poly(ethylene glycol)<sup>25,26</sup> provides a better solution, if applicable, to prevent adverse impact of e-waste of e-textiles at the design stage. PCL was chosen as the biodegradable polymer for this study due to the proven ability to produce nanofibres with good physical properties. Moreover, PCL could be used as an insulating polymer to provide structural stability in humid environments due to its insolubility in water. Hence, the development of PANI/PCL conductive and biodegradable nanofibrous yarn (CBNY) is highly desired in the current context of smart textiles. PANI/PCL conductiving of

Herein, we report on the synthesis and manufacturing of conductive polymer based biodegradable core–shell nanofibrous yarns. The nanofibrous core was prepared by electrospinning PCL and subsequently, aniline was *in situ* polymerized on the surface of the electrospun fibers to form the shell. These conductive and biodegradable nanofibrous yarns (CBNYs) were comprehensively characterized for monomer concentration, morphology, electrical resistance and biodegradability. It is envisaged that this nanofibrous yarn would serve as a short lifecycle substitute for the components of smart textiles eliminating e-waste.

## Experimental

#### Materials and reagents

All chemicals and reagents were analytical grade and used without further purification. Aniline (ACS reagent,  $\geq 99.5\%$ ), dimethylformamide (DMF, ACS reagent,  $\geq 99.8\%$ ), chloroform (CHCl3, 99.8% purity), ethyl alcohol (200 proof, anhydrous, ZerO2®,  $\geq 99.5\%$ ) and polycaprolactone (PCL, average Mn 80 000) were purchased from Sigma Aldrich and used as received. Ammonium persulphate (ammonium peroxydisulphate (APS)) was purchased from Research-Lab Fine Chem Industries. Hydrochloric acid (HCl, extrapure AR 37%) was purchased from Sisco Research Laboratories Pvt. Ltd.

#### Preparation of PANI/PCL nanofibrous yarns

PANI/PCL yarns were prepared by a two-step method. First, an electrospun PCL nanofibrous yarn (PNY) was manufactured. In order to prepare the electrospinning solution, PCL was dissolved in a solvent mixture of DMF and chloroform (volume ratio of DMF : chloroform =1:4) with a concentration of 10% (w/w). A customized electrospinning setup was employed to manufacture PCL yarns (Fig. 1). Two syringes connected to the direct current (DC) high voltage power supply (MATSUDA Precision 0–30 kV) were placed symmetrically on two sides of a grounded funnel. The applied voltages of two needles (diameter =1.2 mm, length =38 mm) were 25 kV and solution flow rate was maintained at  $10\pm2~\mu l$  min $^{-1}$  for both syringes. The distance between the needle tip and collector was maintained 15 cm. Other reported work on conductive nanofibres

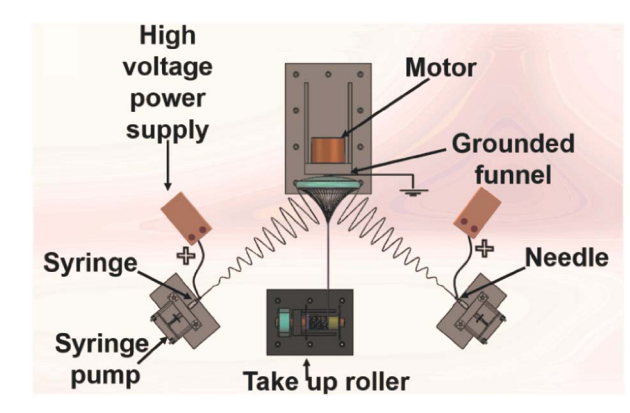


Fig. 1 Schematic of the apparatus for producing continuous twisted varns

has also reported similar distances between the needle tip and the collector.<sup>31</sup> The rotational speed of the funnel and the take-up roller were maintained at 250 rpm and 2 mm min<sup>-1</sup>, respectively. The twist of the yarn was inserted by rotation of the funnel. When the initial cone was formed, a yarn was drawn out towards the take-up roller.

As the second step, PANI layer was synthesized on the surface of PNY by in situ chemical oxidative polymerization of aniline (Fig. 2). The oxidation of aniline monomer was achieved with the help of ammonium persulfate (APS) as the oxidizing agent. In this method, the formed polymer precipitates in the reaction medium and can be deposited in various non-conductive hydrophilic and hydrophobic surfaces.<sup>32</sup> In order to synthesize PANI layer, PNY was wound on a nylon mesh to prepare a PCL yarn skein and then this was immersed in 50 ml aniline/HCl solution which was kept in a mechanical shaker at 100 rpm at room temperature (27 °C) for 30 min. Next, 50 ml of APS/HCL mixture was added dropwise to the solution and agitated in the same conditions for 30 min until the solution became dark green color (Fig. S1†). The higher conversion percentage  $(\sim 90\%)$  of aniline to polyaniline can be obtained by keeping the reaction time for 30 min.33 The monomer, unreacted initiator, and water-soluble oligomers were removed by consecutive washing from 1 M HCl, deionized water, and ethanol. Subsequently, the yarn was washed with 1 M HCl, deionized water, ethanol and dried in a vacuum oven at 30 °C for 4 hours. APS and aniline were mixed with HCL as shown in the Table 1 to vary the aniline concentration.

A custom-made twisting device was prepared as shown in Fig. 3. This device has two sets of clamps of which one set is stationary and the other set is moveable. The device can be further customized by installation of additional clamps as necessary for the required number of plies. The plied yarns were prepared based on self-twist principle to make the yarn attain the mechanical stability to avoid instinctive untwisting. Two pieces of the twisted yarns that were obtained from continuous electrospinning setup were clamped to stationary clamps and the other sides were rotated to provide 'S' and 'S' twist into each of the two strands as shown in Fig. 3(a). When moveable clamps with two twisted strands were brought closer, they immediately

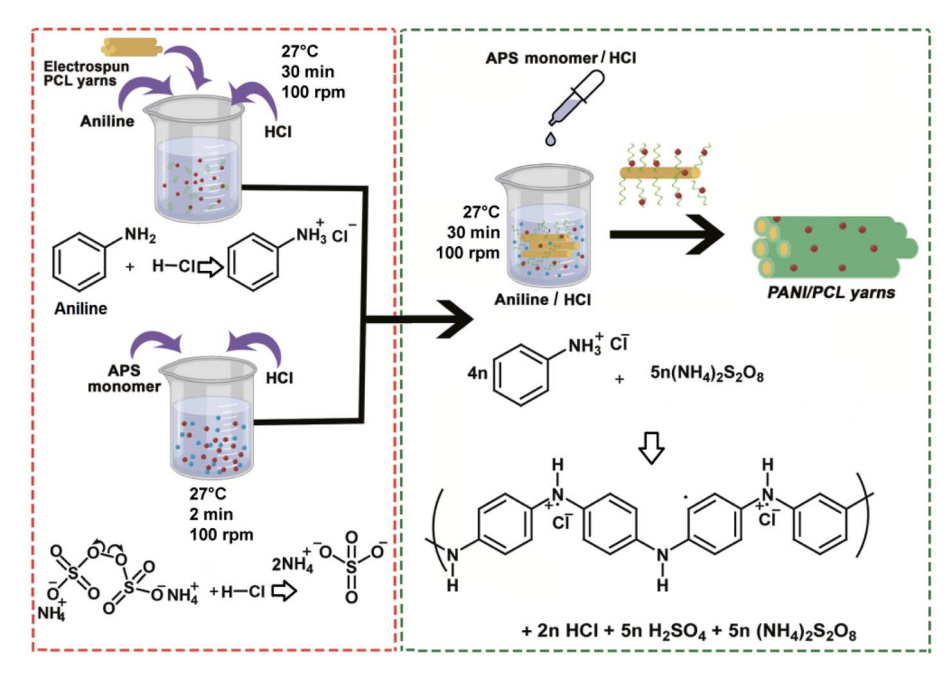


Fig. 2 Schematic illustration of fabrication of PANI decorated PNYs

Table 1 The aniline and APS volumes used for in situ polymerization of aniline

Aniline concentration (v/v %)	HCl concentration (M)	Aniline volume per 50 ml of HCl (μl)	APS weight per 50 ml of HCl (g)
0.5%	0.5	250	0.775
1.0%	1.0	500	1.550
2.0%	2.0	1000	3.100

converged into Z self-twist as shown in Fig. 3(b) and the movable clamps were rotated around the axis of fixed clamps. This process resulted in a twisted yarn of approx. 20 twists per inch. Similarly, three single-ply yarns were twisted into 3-ply yarn by giving Z twist with 10 twists per inch.

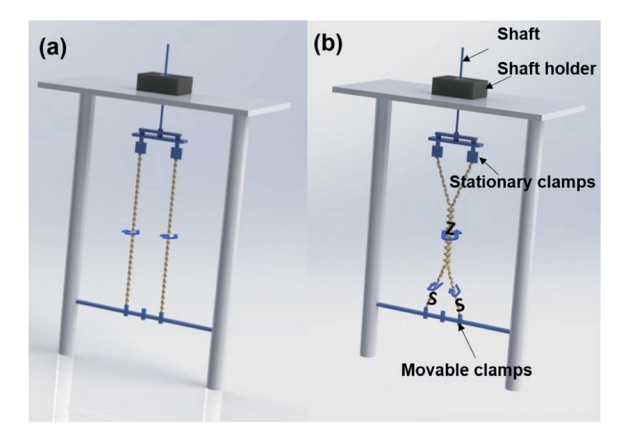


Fig. 3 Schematic diagrams showing the set-up used to further (a) twist single electrospun yarns and (b) twist to produce ply yarns.

#### Characterization methods

The surface topography and morphology of nanofibrous yarns were examined using field emission scanning electron microscope (FESEM), Hitachi SU6600 Analytical Pressure FESEM.

Prior to SEM imaging, the sample surface was coated with a thin gold layer ( $\sim$ 1 nm) using a Hitachi sputter coater device to make the sample surface conductive. The yarn resistance along the yarn length was measured by the two-probe method using (Fluke 289 True-RMS Data Logging Multimeter). The conductive yarn was released from one end and wound from other end as shown in the schematic arrangement in (Fig. S2†). Out of the two probes, one probe was kept stationary and movable probe was dragged along the yarn length by increasing the distance between two probes by 1 cm. In addition, electrical characteristics were measured utilizing a Keithley 2450 SMU four-probe instrument by changing current source between  $-10~\mu$ A to  $+10~\mu$ A.

Differential Scanning Calorimeter (Q2000 DSC from TA Instruments, New Castle DE) was used to determine the thermal properties of PANI/PCL fibers. Samples were heated up to 400 °C in nitrogen atmosphere at a rate of 10 °C min<sup>-1</sup>. Thermogravimetric analysis (TGA) was performed in a nitrogen atmosphere using an STD Q600 instrument. Small pieces of yarn

samples (10–15 mg) was compressed onto an alumina pan that was heated from room temperature to 1000 °C at a heating rate of 20 °C min<sup>-1</sup>. The percentage of weight loss and ash content were derived and studied using TGA curves. The effect of stretching on resistance was measured at variable percentages of displacements from the initial length of the yarn. The strain was applied from 0–400% using a homemade apparatus as shown in Fig. S3.† Then the behaviour of resistance of the device for eight stretch and recovery cycles at 20% strain was studied by measuring the resistance of the device with respect to time.

#### Biodegradation under controlled composting conditions

Biodegradability of PCL and PANi/PCL coated films were tested according to ASTM 5338 standard. The biodegradability was compared against the cellulose filter papers as the positive control and polyethylene plastic sheets as the negative control.

The test specimens were prepared with the dimensions of 25  $\times$  25  $\,\mathrm{mm}^2$  pieces. Water was added to the soil until the overall moisture content becomes 50%. The samples were observed weekly, and the excess liquid was added to maintain constant moisture content. The samples were kept at a temperature of 58  $\pm$  2 °C. Further, the samples were shaken weekly to maintain uniformity. The sample containers were filled up to 75% of the

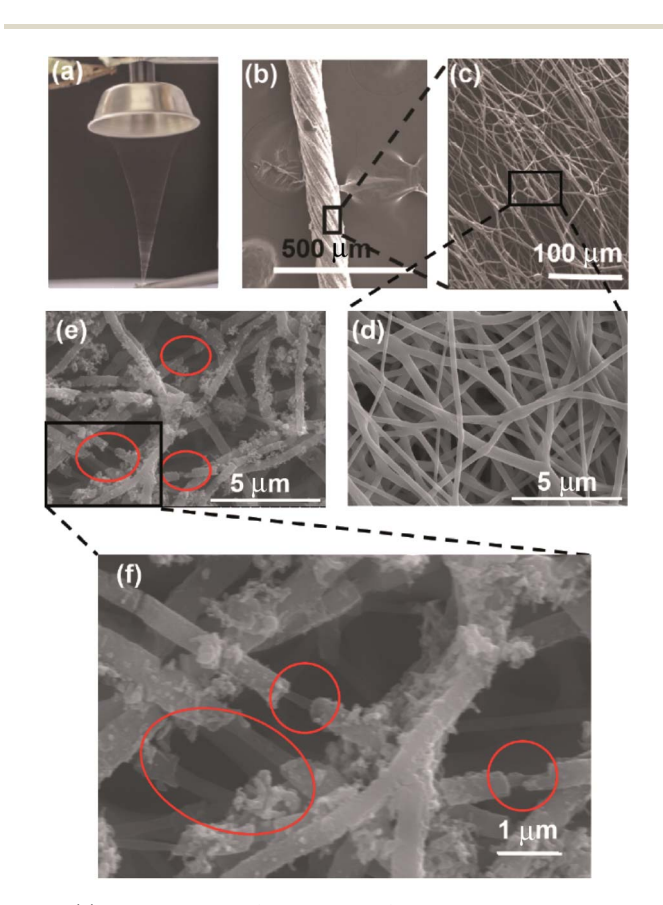


Fig. 4 (a) A photograph of the 3D nanofiber cone drawn out towards the collector and SEM images of (b) twisted yarn (c) aligned PCL nanofibers and (d) magnified image of (c). (e) PANI/PCL core-shell nanofibers and (f) magnified image of (e).

maximum content of specimen and soil.<sup>34</sup> The samples were recovered from compost soil weekly. Then the weight was measured to calculate the weight loss, the change of physical appearance was recorded and reburied. Furthermore, the morphology of degraded PANI nanofiber mats were observed using SEM images.

#### Results and discussion

#### Yarn morphology

The SEM image analysis revealed that electrospun yarns were consisted of twisted fibers (diameter  $=450\pm50$  nm), which were aligned on the direction of the twist (Fig. 4(a–c)). This twist in fibers could have been resulted from the rotation of the funnel while the yarn was drawn out by the take-up roller. Neat PCL yarn morphology exhibited a network of fibers as shown in Fig. 4(d). The broken fiber ends of the PANI/PCL yarns show core–shell morphology (Fig. S4†) where PANI is the shell layer (Fig. 4(e and f)). The yarn itself exhibited an average diameter of  $150\pm6~\mu m$ . When the aniline concentration was increased from 0.5% to 2%, the fiber diameter of composite fibers was increased from  $443\pm62$  nm for pure PCL to  $457\pm83$  nm for 0.5% aniline,  $468\pm63$  nm for 1% aniline and  $554\pm73$  nm for

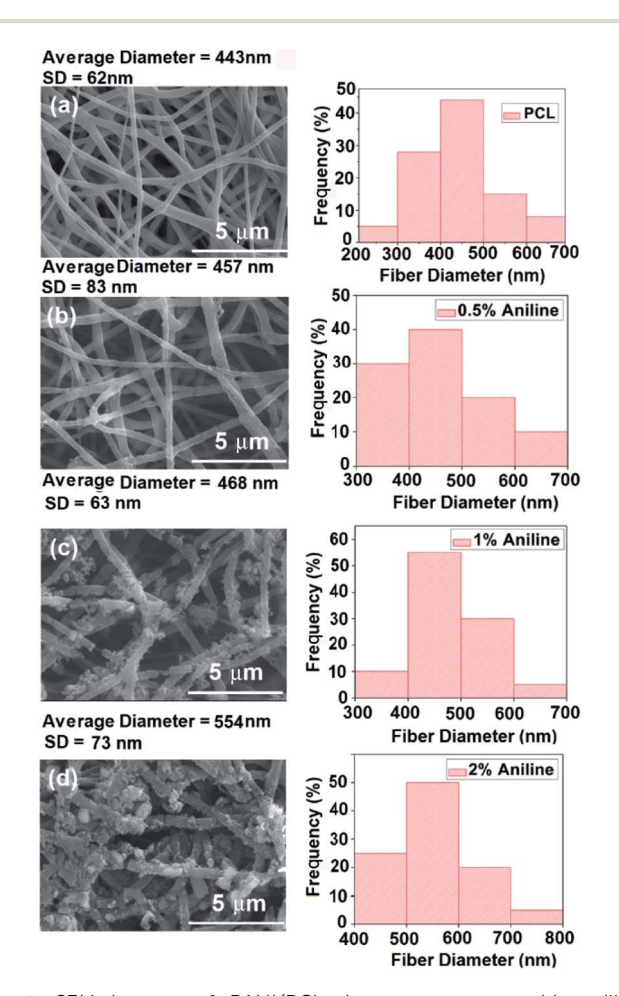


Fig. 5 SEM images of PANI/PCl electrospun mats with aniline concentrations of (a) 0%, (b) 0.5%, (c) 1.0%, (d) 2.0%.

Paper

Sesistance Der Unit Length (kD/cm)

150

120

90

0.5

1.0

1.5

2.0

Concentration of Aniline (v/v %)

Fig. 6 Variation of resistance per unit length as a function of aniline concentration.

2% aniline, respectively (Fig. 5). A discontinuous thin layer of PANI shell layer was observed on the surface of PCL fibers for low concentrations of aniline (0.5%) while small clusters of PANI started forming on the surface of PCL fibers and more PANI coverage of fiber surface was noticed for 1% aniline concentration. The size and the number of clusters increased with the initial monomer concentration leading to full coverage of the fiber (Fig. 5(a–d)). The pores between the fibers were observed to be occupied by PANI polymerized from the highest concentration of aniline. The average diameter of nanofibers has increased by about  $\sim\!\!100$  nm with the deposition of the PANI layer with 2% aniline concentration.

#### Electrical resistance of yarns

The electrical resistance of CBNYs was measured. The electrical resistance of the yarns was decreased from  $162\pm15~\mathrm{k}\Omega~\mathrm{cm}^{-1}$  to  $6\pm10~\mathrm{k}\Omega~\mathrm{cm}^{-1}$  for yarns coated with initial aniline concentrations of 0.5% and 2%, respectively (Fig. 6). Furthermore, the *I–V* characteristics (Fig. S5†) of the CBNYs were recorded. The voltage *versus* current shows a steady increment and when the aniline concentration was increased from 0.5% to 2%, the gradient of the graph was decreased indicating the declining resistance. The *I–V* response has been shown to be vital in measuring the changes of current due to availability of electrons in materials.<sup>35</sup>

The electrical conductivity of PANI results from decolonization of electrons through the  $\pi$ -conjugated system.<sup>36</sup> Furthermore, HCl could act as a dopant to protonate PANI in the emeraldine base (EB) form to the emeraldine salt during polymerization. It was reported that protonation decreases the HOMO–LUMO gap (band gap).<sup>37</sup> Other factors affecting the electrical resistance of PANI coated nanofibers are the morphology of the coated polymer and the degree of doping. When considering the morphology, it is clear that at the lowest concentrations (aniline 0.5%), the conductive path may be disturbed by the discontinuities of PANI deposition observed on the yarn surface. This separation of deposited particles may not

allow the transportation of electrons between them.<sup>38</sup> When the concentration was doubled as aniline 1%, increased PANI coverage was observed on the fibers. This morphology of thick, uniform PANI deposition layer may have been responsible for forming continuous conductive network with a higher surface charge density, which allowed efficient charge transport on the surface of the yarn enabling higher conductivity. Further increase of aniline concentration (aniline 2%) lead to the lowest electrical resistance of yarns due to thick PANI coverage as shown in SEM images in Fig. 5. However, 2% aniline presented a higher standard deviation of the resistance values that may be attributed to several factors. First of all, the structural defects on the fiber due to short-term degradation of PCL caused by the hydrolysis of polymer backbone<sup>39,40</sup> may have influenced the traffic of electrons leading to a higher variation of resistance values. Secondly, the uneven deposition of PANI on the surface of fibers and islands of PANI agglomeration from sample to sample may have resulted in resistance values with higher variation.

The degree of doping is another significant factor affecting the resistance values of the PCL/PANI fibers. Conductivity is

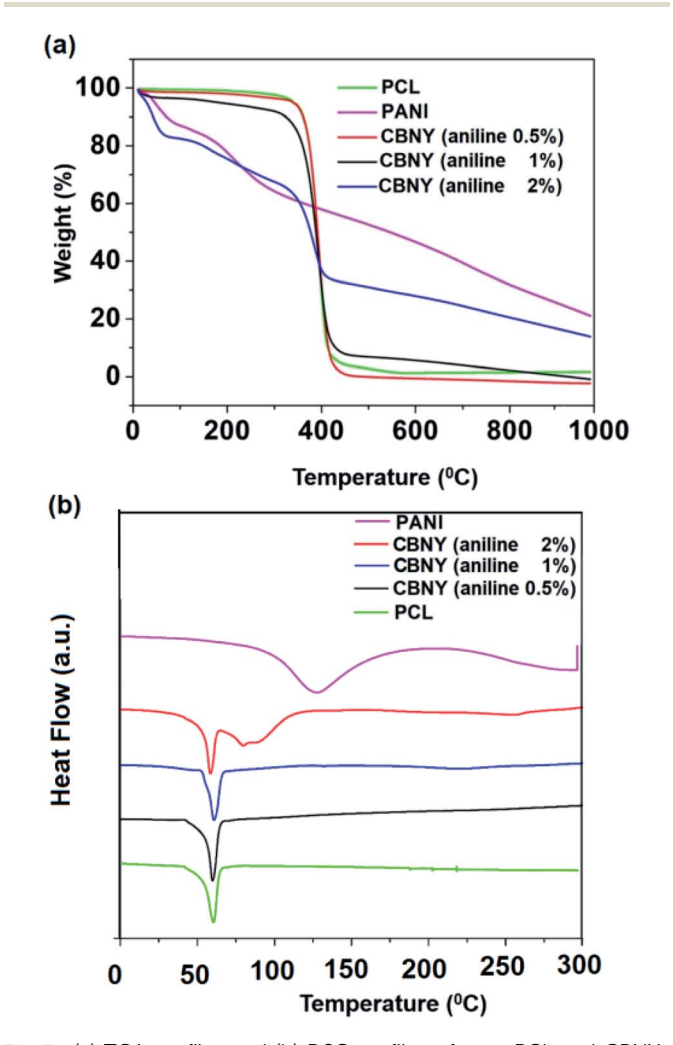


Fig. 7 (a) TGA profiles and (b) DSC profiles of pure PCL and CBNYs (polymerized from aniline 0.5%, 1% and 2%).

found to increase proportionally with the amount of dopant used.<sup>41</sup> For low concentrations of aniline, the H<sup>+</sup> dopant concentration was low, resulting in polymerization of structured "tail–tail", "head–head", adducts, which could affect a decline in the electrical conductivity of polyaniline. When the H<sup>+</sup> concentration was high, polymerization of aniline formed the usual "head–tail" connections leading to lower resistivity values as observed in this experiment.<sup>42</sup>

#### Thermal properties of PANI/PCL yarns

Thermal properties of PANI/PCL yarn were investigated using thermogravimetric analysis (TGA) and Differential Scanning Calorimetric (DSC) analysis as shown in Fig. 7. TGA curves exhibited weight loss occurring due to loss of water, HCl and other volatile solvents between 0–120 °C. <sup>43</sup> This weight loss was increased with the increasing PANI content that may be attributed to the increased water content due to the readily formation of hydrogen bonds with doped PANI during the polymerization. <sup>44</sup> Therefore, the first weight loss may be considered as a good indication for content of PANI in PANI/PCL yarns.

The next main degradation event occurred at an onset temperature between 374–389 °C (see Table 2) which can be attributed to the degradation of PCL. The onset temperature of PCL degradation was found to be decreasing from 386 °C for pure PCL to 374 °C for PANI/PCL yarn polymerized from 2% aniline. Thermal stability of PCL/PANI yarns was investigated by comparing the temperatures resulting in 95% residual weight of sample. Thermal stability was found to be decreasing with the increasing aniline concentration. The PANI coated PCL composites revealed a higher amount of residue with the increase of PANI content in the composite. This indicated that PANI acted as a protective barrier on the surface of PCL against thermal degradation in PANI/PCL composite membranes.<sup>45</sup> Overall, TGA analysis indicated that PANI in PANI/PCL yarn has

a significant influence on thermal properties of PCL/PANI composite yarns and the thermal stability has decreased with the increasing PANI content.

Melting temperature  $(T_{\rm m})$  and melting enthalpy  $(\Delta H_{\rm m})$  were determined from the DSC heating thermograms of PCL/PANI yarns as shown in Fig. 7(b). The endothermic peak of pure polyaniline at  $\sim$ 126 °C could be attributed to the evaporation of water bound to the PANI crystal lattice. This can be related to the weight loss observed in the TGA curves. A broad endothermic peak of CBNY (aniline 2%) at  $\sim$ 80 °C has emerged next to the melting peak of PCL. This peak may represent the endothermic peak of PANI itself shifting downward from the position observed for pure PANI. This observation confirms the presence of PANI on the surface of PCL yarn and the downward shift of the peak may indicate the presence of smaller crystals.

The DSC thermogram of neat PCL yarn showed a peak corresponding to 60 °C with an enthalpy of 72 J g $^{-1}$  that can be attributed to the melting of PCL. This melting enthalpy ( $\Delta H_{\rm m}$ ) of PCL was decreased to 51 J g $^{-1}$  for CBNY (aniline 1%) and to 37 J g $^{-1}$  (aniline 2%) which could be attributed to two factors; first, the presence of acid may have hydrolysed the crystal structure of PCL and secondly, deposition of PANI may have created defects in the PCL crystal structure leading to reduced melting enthalpy. Furthermore, the  $T_{\rm m}$  of PCL decreased from 61 °C for pure PCL to 58 °C for PANI/PCL nanofibrous yarns. The reduction of thermal stability (Table 2) and the percentage of crystallinity (Table 3) were also observed supporting the idea that either the size of PCL crystals has been reduced or creation of crystal defects has taken place due to the hydrolysis of PCL in presence of PANI and HCl. $^{47}$ 

#### Electromechanical behaviour of plied yarns

PCL/PANI nanofibrous yarn with PANI polymerized from 1% aniline solution (CBNY-aniline 1%) was selected for further

Table 2 TGA data compilation including the weight loss attributed to HCL and water, onset and weight loss attributed to PCL, residual weight, and thermal stability of PANI/PCL nanofibers (polymerized from aniline 0.5%, 1% and 2%)

Sample	Weight loss due to HCl (%)	Onset temp. of PCL (°C)	Weight loss of PCL (%)	Residual weight (%)	Thermal stability (°C)
PCL pure	_	386	98	2	356
Aniline 0.5%	3	389	96	1	252
Aniline 1%	7	378	89	4	188
Aniline 2%	16	374	54	30	96
PANi powder	13	_	_	44	65

Table 3 Melting temperature, melting enthalpy and percentage crystallinity of pure PCL and CBNYs (polymerized from aniline 0.5%, 1% and 2%)

Sample	Melting temperature of PCL $(T_{\rm m}, {}^{\circ}{\rm C})$	Melting enthalpy PCL ( $\Delta H_{ m m}$ , J $ m g^{-1}$ )	Percentage crystallinity (%)
PCL pure	61	72	52
Aniline 0.5%	60	69	49
Aniline 1%	61	51	37
Aniline 2%	59	37	27

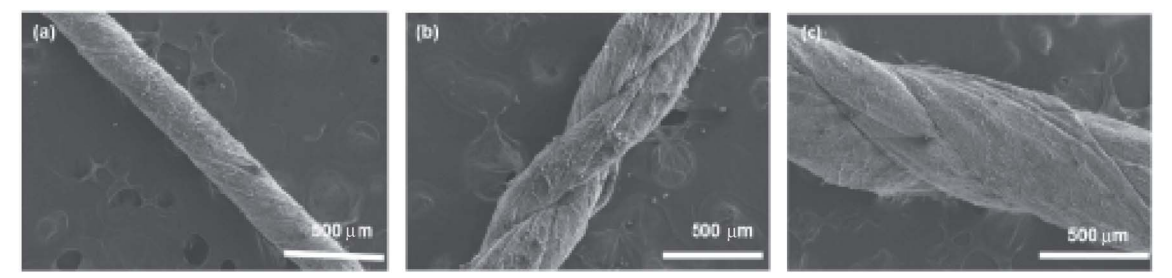


Fig. 8 SEM images of the CBNYs (a) single ply, (b) 2-ply, (c) 3-ply

investigation of electromechanical properties. Two sets of plied yarns were manufactured as in two-ply yarn and three-ply yarn. The plied yarns were manufactured with the fiber alignment (Fig. 8(a-c)) along the direction of the twist such that this could favourably contribute toward the tensile strength of the fibers. The electrical resistance of the plied yarns were investigated by measuring the resistance per unit length. The increase in number of plies to three has resulted in a decrease in resistance as shown in Fig. 9. This could be explained by two approaches and firstly, the increase of cross-sectional area with the number of plies may have resulted in lower resistance. Secondly, the mechanism of conductivity of conductive polymers may hold a key to this reduction of resistance. Bulk conductivity in the polymer material depends on the need for the electrons to jump from one polymer molecule to the adjacent molecule, which is also identified as an intermolecular charge transfer reaction. Furthermore, the conductivity is determined by the macroscopic factors like poor contacts between different crystalline regions in the material. When the number of plies of the yarn is increased to three, it can be assumed that more number of contacts between regions of fibers were established facilitating intermolecular charge transfer, and thus decreasing the electrical resistance. The yarns are typically subjected to strain in wearable applications such as garments. The variation of electrical resistance as a function of applied strain was investigated to determine the suitability of this CBNY (aniline 1%) for the

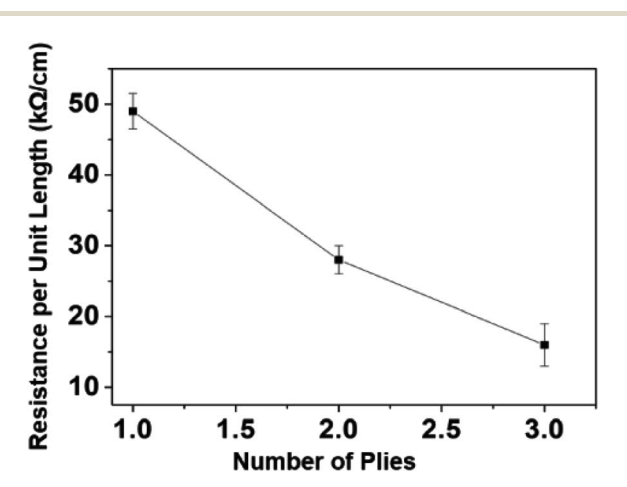


Fig. 9 Variation of resistance as a function of number of plies on resistance.

intended wearable applications (Fig. 10(a)). The electrical resistance increased exponentially with the applied strain on yarn. This can be attributed to the inhibition of electron transfer process from one molecule to another molecule due to lack of contact between crystal regions of PANI. Yarn stretching process may break the crystal regions resulting in an increase of distance between those regions making it difficult for the intermolecular charge transfer to take place. Wearable applications envisaged for this yarn are subjected to constant stretch and recovery cycles arising from body movements. The electrical resistance of PCL/PANI yarn for seven repeated stretch-

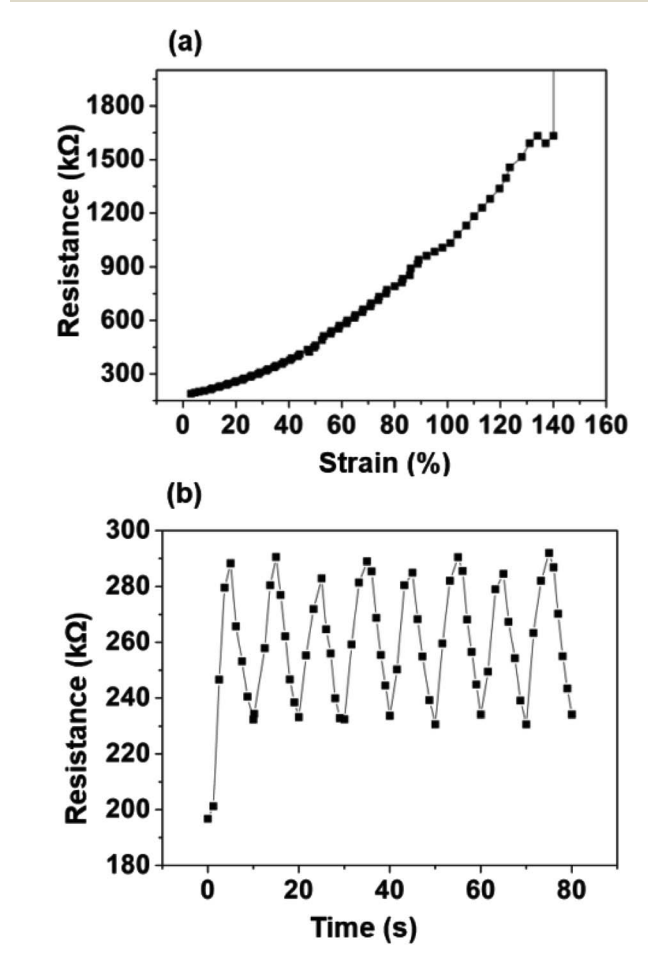


Fig. 10 (a) Variation of resistance with applied tensile strain of yarn. (b) Time dependent normalized resistance change of the yarn for multiple stretch–recovery cycles (maximum strain of 20%).

recovery cycles was measured (Fig. 10(b)). The yarns were stretched up to 20% strain and released at a controlled displacement rate. The yarns exhibited an increase of resistance during stretch and a decrease of resistance during recovery. The rate of increase and decrease was observed to be consistent for all stretch–recovery cycles demonstrating the excellent repeatability of this process. This can be attributed to the continuous coverage of the PCL fiber surface by polyaniline ensuring that the conductive pathways were not easily disturbed at 20% strain. Interestingly, the resistance changes almost instantaneously with the stretch for multiple stretch and recovery cycles. This rapid and sensitive response to mechanical loading and unloading is promising to validate the possibility of using the CBNYs as strain sensors for human motion monitoring.

#### Weaving

To demonstrate the ability to incorporate this yarn into fabrics, weaving was successfully performed as shown in Fig. 11(a-c). A two-ply conventional polyamide yarns were used as weft (widthwise) in the woven structure, while the PCL/PANI conductive plied yarns were being used as the warp (lengthwise) yarns. Electrical resistance of a length of 1.5 cm of warp yarn in the fabric was measured to be 80.1 k $\Omega$  (Fig. S6(a)†). Furthermore, the plied yarn was fed into a sewing needle and was stitched onto a polyamide fabric successfully (Fig. 11(d-f)). It was verified that the yarn was mechanically strong enough to be sewn with a sewing needle. The PCL/PANI conductive yarn sewn into fabric with a length of 40 mm has indicated a resistance of 197.9 k $\Omega$  (Fig. S6(b)†). The calculated resistance per unit length was  $\sim 50 \text{ k}\Omega \text{ cm}^{-1}$  for both sewn and woven yarn. Hence, it is clear that the conductive polymeric layer remains undamaged with mechanical deformation of material during sewing and weaving.

#### Fabrication of a capacitive sensor

As a proof-of-concept, a capacitive sensing device was fabricated by sewing the CBNY (aniline 1%) into a fabric as an electrode for

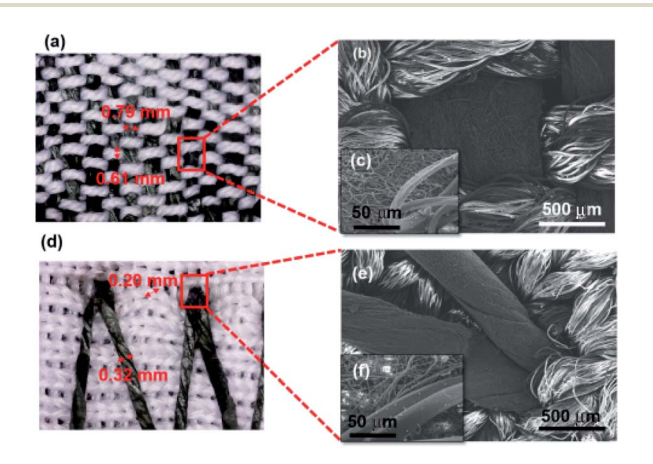


Fig. 11 (a) Optical microscopic image of a fabric woven with PCL/PANI composite and polyamide yarns, (b and c) SEM images of the woven fabric. (d) Optical microscopic image of the sewn yarn, (e and f) SEM images of the sewn yarn.

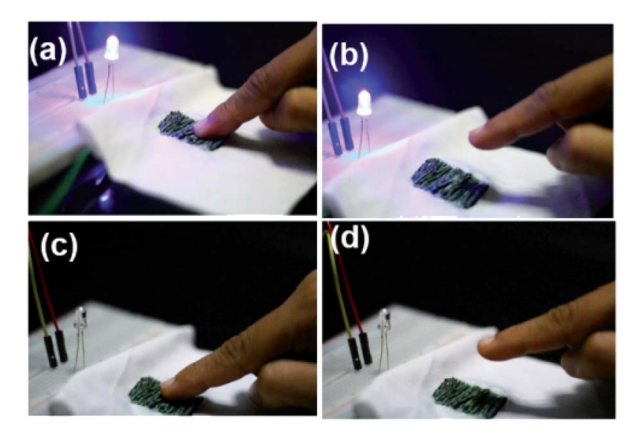


Fig. 12 Illustration of the electrical conductivity nature for the prepared CBNYs with application of flexible capacitive sensor for operation of LED (a) ON by touching, (b) unchanged by releasing, (c) OFF and (d) unchanged by releasing.

capacitive sensing applications (Fig. 12(g-i)). The LED bulb can be turned ON using one touch by finger and turned OFF by a consecutive another touch. Likewise, the LED bulb can be turned ON and OFF by touching on the flexible fabric electrode (see ESI†).

#### **Biodegradability**

Biodegradation potential of PCL/PANI films were investigated as per the ASTM 5338 standard using a laboratory compost system. Composite specimens were recovered from compost

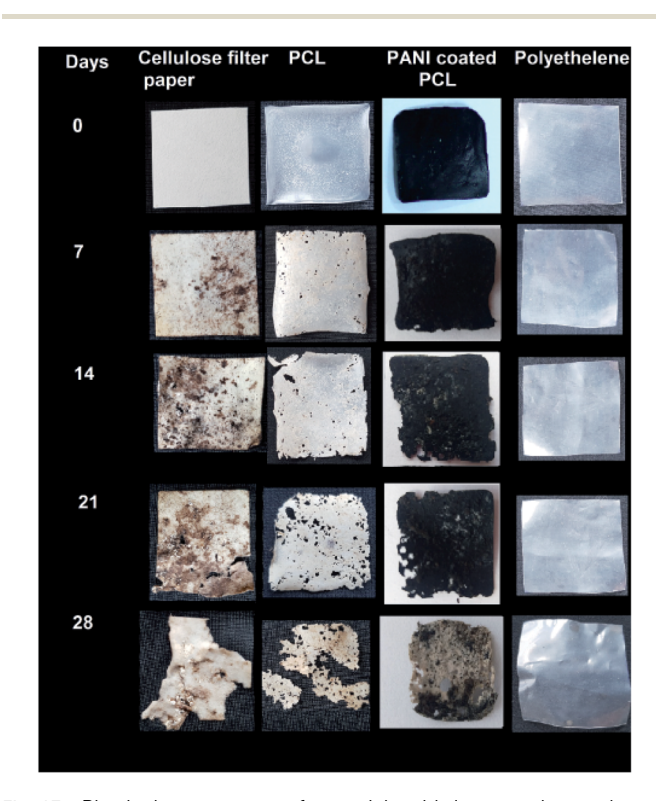


Fig. 13 Physical appearance of materials with increase in number of days of composting.

soil at various levels of degradation. Composting is the most observed to be depractical and preferable disposal route for biodegradable observed to be depractical and preferable disposal route for biodegradable observed to be depractical and preferable disposal route for biodegradable observed to be depractical and preferable disposal route for biodegradable observed to be depractical and preferable disposal route for biodegradable observed to be depractical and preferable disposal route for biodegradable observed to be depractical and preferable disposal route for biodegradable observed to be depractical and preferable disposal route for biodegradable observed to be depractical and preferable disposal route for biodegradable observed to be depractical and preferable disposal route for biodegradable observed to be depractical and preferable disposal route for biodegradable observed to be depractical and preferable disposal route for biodegradable observed to be depractical and preferable disposal route for biodegradable observed to be depractical and preferable disposal route for biodegradable observed to be depractical and preferable disposal route for biodegradable observed to be depractical and preferable disposal route for biodegradable observed to be depractically disposal route for biodegradable observed to be dependent of the depractical disposal route for biodegradable disposal route for

practical and preferable disposal route for biodegradable products. PCL is found to degrade gradually at a temperature of 58 °C and a humidity condition of 60%. Degradation of PCL may take place in various eco-systems such as water, soil, and compost. Here, degradation of PCL may take place in various eco-systems such as water, soil, and compost. Here, degradation of PCL in compost can be based on typical modes of chemical and biological degradation through chemical hydrolysis of ester bonds and enzymatic attack, respectively.48 PCL can be degraded by several enzymes by either the action of aerobic or anaerobic microorganisms.49 It can be observed that PCL/PANI degradation was started by sample embrittlement as early as one week (Fig. 13). A strong correlation was shown to exist between the physical changes in surface morphology and weight loss percentage (Fig. 14) of films. The degraded films showed more ruptures, grooves, pores, cavities, grooves of nanofibrous surface (Fig. S7†).

The first phase of degradation process can be driven from biological and physical forces, which can result in mechanical damage such as polymeric fragmentation and cracking. Furthermore, PCL degradation can be taken place by both surface and bulk erosion. Bulk erosion entails water penetration throughout the material and degrade the entire structure simultaneously, whereas surface erosion is limited only to the specimen surface with a constant rate of degradation.<sup>50</sup> Since enzymatic degradation generally occurs on the polymer surface, in the compost environment, the surface erosion may be prominent for PCL due to hydrolytic enzymes. This may be the reason for exhibiting a constant degradation rate by PCL compared to PANI coated PCL.<sup>51</sup> In contrast, bulk erosion<sup>52</sup> may be prominent for PANI coated PCL, in which nearly constant dimension was shown until third week and the surface erosion might be inhibited by non-biodegradable PANI layer. However, water diffusion into interior may have occurred to though mechanical damages of PANI coating, which can support chain cleavage and detachment of PANI coating. Although PANI is a non-biodegradable polymer, the ultrathin coating of PANI was

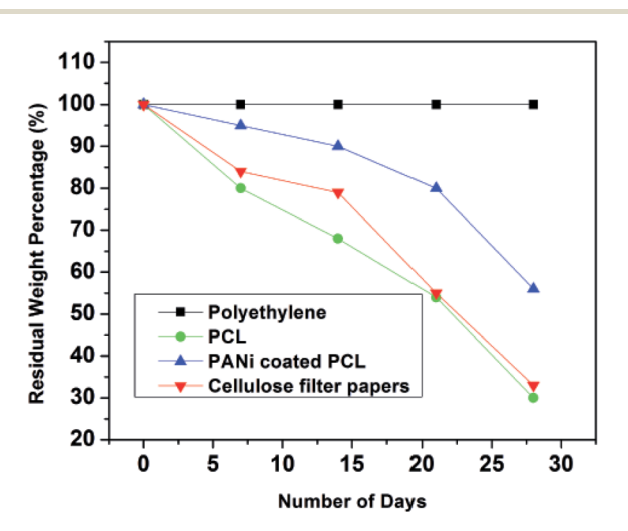


Fig. 14 Residual weight percentage as a function of number of days.

observed to be detaching from PCL core with degradation of PCL after four weeks. Finally, a rapid increment in degradation can be detected after 21 days of time due to removal of PANI layer. PCL/PANI exhibited a slower degradation rate compared to pure PCL.

#### Conclusion

In conclusion, we have explored the initial design and fabrication of all-organic conductive and biodegradable yarn with instantaneous electrical response to change of strain. Electrospun PNYs were decorated with *in situ* polymerization of aniline. Increasing the concentration of aniline in the reaction mixture resulted in a decrease of resistivity in PCL/PANI yarns. The thermal analysis indicated the reduction of the melting enthalpy in the presence of PANI. The electrical resistance of yarns was measured for different applications including plied yarns, woven fabrics, and sewn yarns where yarn can be subjected to mechanical deformations. Furthermore, the application of the yarn as a wearable sensor was demonstrated by fabricating a capacitor device. The composite yarns exhibited biodegradability as a short life cycle substitutes for the components of an electronic device minimizing the e-waste.

### Conflicts of interest

The authors declare no conflict of interest.

## Acknowledgements

The authors would like to acknowledge the Senate Research Council, University of Moratuwa for funding the project under the SRC Grant (SRC/LT/2018/33). The authors gratefully acknowledge Sri Lanka Institute of Nanotechnology for providing advanced laboratory resources.

#### References

- 1 M. Stoppa and A. Chiolerio, Sensors, 2014, 14, 11957-11992.
- 2 S. Park and S. Jayaraman, MRS Bull., 2003, 28, 585-591.
- 3 R. Salvado, C. Loss, R. Gonçalves and P. Pinho, Sensors, 2012, 12, 15841–15857.
- 4 C. Cochrane, V. Koncar, M. Lewandowski and C. Dufour, *Sensors*, 2007, 7, 473–492.
- 5 H. Chen, K. Lee, J. Lin and M. Koch, *J. Mater. Process. Technol.*, 2007, **192**, 549–554.
- 6 B. Farrell, P. W. Nguyen, J. Teverovsky, J. Slade and M. Powell, Method of manufacturing a fabric article to include electronic circuitry and an electrically active textile article, US Pat., 6729025, 2004.
- 7 A. Yetisen, H. Qu, A. Manbachi, H. Butt, M. Dokmeci, J. Hinestroza, M. Skorobogatiy, A. Khademhosseini and S. Yun, ACS Nano, 2016, 10, 3042–3068.
- 8 K. R. Dandekar, G. Dion, A. K. Fontecchio, T. P. Kurzweg, D. Patron and O. Montgomery, Smart knitted fabrics, *US Pat.*, 2016/0000374.A1, 2016.

- 9 R. Paradiso, L. Caldani and M. Pacelli, in *Wearable Sensors*, Elsevier, 2014, pp. 153–174.
- 10 B. Wu, B. Zhang, J. Wu, Z. Wang, H. Ma, M. Yu, L. Li and J. Li, *Sci. Rep.*, 2015, 5, 11255.
- 11 H. Bai and G. Shi, Sensors, 2007, 7, 267-307.
- 12 N. K. Guimard, N. Gomez and C. E. Schmidt, *Prog. Polym. Sci.*, 2007, **32**, 876–921.
- 13 A. G. MacDiarmid, Angew. Chem., Int. Ed., 2001, 40, 2581–2590.
- 14 B. Kim, V. Koncar and C. Dufour, *J. Appl. Polym. Sci.*, 2006, **101**, 1252–1256.
- 15 S. Palaniappan and A. John, *Prog. Polym. Sci.*, 2008, **33**, 732–
- 16 B. Zhang, F. Kang, J.-M. Tarascon and J.-K. Kim, *Prog. Mater. Sci.*, 2016, 76, 319–380.
- 17 P. Gibson, H. Schreuder-Gibson and D. Rivin, *Colloids Surf.*, A, 2001, 187, 469–481.
- 18 W. E. Teo and S. Ramakrishna, *Nanotechnology*, 2006, **17**, R89.
- 19 Y. Zhou, J. Fang, X. Wang and T. Lin, *J. Mater. Res.*, 2012, 27, 537–544.
- 20 D. Aussawasathien, J.-H. Dong and L. Dai, Synth. Met., 2005, 154, 37–40.
- 21 X. You, J. He, N. Nan, X. Sun, K. Qi, Y. Zhou, W. Shao, F. Liu and S. Cui, *J. Mater. Chem. C*, 2018, **6**, 12981–12991.
- 22 S. Wu, P. Liu, Y. Zhang, H. Zhang and X. Qin, Sens. Actuators, B, 2017, 252, 697–705.
- 23 P. Weerasinghe, N. D. Wanasekara, D. Dissanayake, H. R. T. Banadara, N. Tissera, R. Wijesena, K. de Silva and A. Karalasingam, Thailand, *IEEE 14th International Conference on Nano/Micro Engineered and Molecular Systems* (NEMS), 2019, pp. 308–311.
- 24 P. T. Anastas and J. B. Zimmerman, *Environ. Sci. Technol.*, 2003, 37, 94A–101A.
- 25 E. H. Sanders, R. Kloefkorn, G. L. Bowlin, D. G. Simpson and G. E. Wnek, *Macromolecules*, 2003, 36, 3803–3805.
- 26 J. Zeng, X. Xu, X. Chen, Q. Liang, X. Bian, L. Yang and X. Jing, J. Controlled Release, 2003, 92, 227–231.
- 27 R. Sarvari, B. Massoumi, M. Jaymand, Y. Beygi-Khosrowshahi and M. Abdollahi, *RSC Adv.*, 2016, **6**, 19437– 19451
- 28 K. Low, N. Chartuprayoon, C. Echeverria, C. Li, W. Bosze, N. V. Myung and J. Nam, *Nanotechnology*, 2014, 25, 115501.
- 29 A. R. Köhler, L. M. Hilty and C. Bakker, *J. Ind. Ecol.*, 2011, **15**, 496–511.
- 30 A. R. Köhler, Mater. Des., 2013, 51, 51-60.

- 31 S. Veeralingam, A. N. K. Ravindranath and S. Badhulika, *Adv. Mater. Interfaces*, 2020, 2000568.
- 32 S. Fedorova and J. Stejskal, Langmuir, 2002, 18, 5630-5632.
- 33 N. Y. Abu-Thabit, J. Chem. Educ., 2016, 93, 1606-1611.
- 34 H. Y. Sintim, A. I. Bary, D. G. Hayes, L. C. Wadsworth, M. B. Anunciado, M. E. English, S. Bandopadhyay, S. M. Schaeffer, J. M. DeBruyn and C. A. Miles, *Sci. Total Environ.*, 2020, 138668.
- 35 S. Veeralingam and S. Badhulika, *Mater. Sci. Eng.*, C, 2020, 108, 110365.
- 36 S. Islam, G. Lakshmi, A. M. Siddiqui, M. Husain and M. Zulfequar, *Int. J. Polym. Sci.*, 2013, DOI: 10.1155/2013/ 307525.
- 37 R.-X. Wang, L.-F. Huang and X.-Y. Tian, J. Phys. Chem. C, 2012, 116, 13120–13126.
- 38 V. Anju and S. K. Narayanankutty, AIP Adv., 2016, 6, 015109.
- 39 A. R. Hernández, O. C. Contreras, J. C. Acevedo and L. Moreno, *Am. J. Polym. Sci.*, 2013, 3, 70.
- 40 A. Haryńska, J. Kucinska-Lipka, A. Sulowska, I. Gubanska, M. Kostrzewa and H. Janik, *Materials*, 2019, **12**, 887.
- 41 A. Kaynak, L. Rintoul and G. A. George, *Mater. Res. Bull.*, 2000, 35, 813–824.
- 42 J. Hong, Z. Pan, M. Yao and X. Zhang, *Synth. Met.*, 2014, **193**, 117–124.
- 43 M. A. C. Mazzeu, L. K. Faria, A. d. M. Cardoso, A. M. Gama, M. R. Baldan and E. S. Gonçalves, *J. Aerosp. Technol. Manage.*, 2017, 9, 39–47.
- 44 W. Łużny and K. Piwowarczyk, *Polimery*, 2011, **56**, 652–656.
- 45 L. Yue, Y. Xie, Y. Zheng, W. He, S. Guo, Y. Sun, T. Zhang and S. Liu, *Compos. Sci. Technol.*, 2017, **145**, 122–131.
- 46 B. Lubentsov, O. Timofeeva, S. Saratovskikh, V. Krinichnyi, A. Pelekh, V. Dmitrenko and M. Khidekel, *Synth. Met.*, 1992, 47, 187–192.
- 47 G. Kale, R. Auras and S. P. Singh, *J. Polym. Environ.*, 2006, **14**, 317–334.
- 48 F. Lefebvre, A. Daro and C. David, J. Macromol. Sci., Part A: Pure Appl. Chem., 1995, 32, 867–873.
- 49 T.-K. Chua, M. Tseng and M.-K. Yang, *AMB Express*, 2013, 3, 8.
- 50 J. Tamada and R. Langer, *Proc. Natl. Acad. Sci. U. S. A.*, 1993, **90**, 552–556.
- 51 K. Krasowska, A. Heimowska and M. Morawska, 1st International Conference on the Sustainable Energy and Environment Development, (SEED 2016), Poland, 2016.
- 52 L. N. Woodard and M. A. Grunlan, *ACS Macro Lett.*, 2018, 7, 976–982.